Eloy Martinez-Heras[1a*] PhD, Francesco Grussu[2,3a] PhD, Ferran Prados[3,4,5] PhD, Elisabeth Solana[1] PhD, Sara Llufriu[1] MD, PhD.

[1]Center of Neuroimmunology, Laboratory of Advanced Imaging in Neuroimmunological Diseases, Hospital Clinic Barcelona, Institut d'Investigacions Biomèdiques August Pi i Sunyer (IDIBAPS) and Universitat de Barcelona. Barcelona. Spain.

[2]Radiomics Group, Vall d'Hebron Institute of Oncology, Vall d'Hebron Barcelona Hospital Campus, Barcelona, Spain

[3]Queen Square MS Centre, Queen Square Institute of Neurology, Faculty of Brain Sciences, University College London, London, UK

[4]Centre for Medical Image Computing (CMIC), Department of Medical Physics and Bioengineering, University College London, London, UK.

[5]E-health Centre, Universitat Oberta de Catalunya. Barcelona. Spain.

[a]These authors contributed equally to this work (co-first authors)

*Corresponding author: Eloy Martinez-Heras. Hospital Clinic Barcelona, Calle Villarroel 170, 08036 Barcelona, Spain. Phone: +34 932275414. Fax: +34 932275783. E-mail: emartind@clinic.cat.

Abstract

Quantitative diffusion imaging techniques enable the characterization of tissue microstructural properties of the human brain "in vivo", and are widely used in neuroscientific and clinical contexts. In this review, we present the basic physical principles behind diffusion imaging and provide an overview of the current diffusion techniques, including standard and advanced techniques as well as their main clinical applications. Standard diffusion tensor imaging (DTI) offers sensitivity to changes in microstructure due to diseases and enables the characterization of single fiber distributions within a voxel as well as diffusion anisotropy. Nonetheless, its inability to represent complex intravoxel fiber topologies and the limited biological specificity of its metrics motivated the development of several advanced diffusion MRI techniques. For example, high-angular resolution diffusion imaging (HARDI) techniques enabled the characterization of fiber crossing areas and other complex fiber topologies in a single voxel and supported the development of higher-order signal representations aiming to decompose the diffusion MRI signal into distinct microstructure compartments. Biophysical models, often known by their acronym (e.g., CHARMED, WMTI, NODDI, DBSI, DIAMOND) contributed to capture the diffusion properties from each of such tissue compartments, enabling the computation of voxel-wise maps of axonal density/morphology that hold promise as clinically viable biomarkers in several neurological and neuroscientific applications; for example, to quantify tissue alterations due to disease or healthy processes. Current challenges and limitations of state-of-the-art models are discussed, including validation efforts. Finally, novel diffusion encoding approaches (e.g., b-tensor or double diffusion encoding) may increase the biological specificity of diffusion metrics towards intra-voxel diffusion heterogeneity in clinical settings, holding promise in neurological applications.

Diffusion-Weighted Imaging: Recent Advances and Applications

1. **Introduction**

1.1. Water diffusion

The noninvasive quantification of tissue microstructure has been largely investigated over the last years using diffusion-weighted Magnetic Resonance Imaging (DW-MRI). DW-MRI exploits biological water, ubiquitous in living tissues, as a non-invasive probe of cytoarchitecture at the mesoscale (1-100 μm). Water molecules constantly undergo random fluctuations of their spatial position according to the well-known phenomenon of Brownian motion. [1] The intrinsic water self-diffusion coefficient characterizes such a phenomenon so that the average mean squared displacement of freely diffusion molecules in N dimensions over a time τ can be calculated via Einstein's relation:

$$<r^2> = 2N\,D\,\tau\ (1).$$

However, in biological tissues, water molecules do not diffuse freely, since Brownian motion happens within complex microenvironments (e.g., cell membranes) that hinder and/or restrict molecule random walks. Consequently, the effective mean squared displacement $<r^2>$ departs (i.e. is reduced) from the free diffusion behavior, and diffusion patterns carry a signature of the cellular characteristics where diffusion occurs.

1.2 Linking diffusion and MRI signals

DW-MRI utilizes magnetic field gradients to sensitize the MRI signal to such patterns of diffusion so that key cellular characteristics that drive these patterns (e.g., cell size, density, morphology) can be estimated from sets of diffusion-sensitized MRI measurements. In the classical DW-MRI experiment, [2] known as pulsed-gradient spin-echo (PGSE) or single diffusion encoding and illustrated in Figure 1 below, two different diffusion-sensitizing pulsed gradient lobes are used to obtain diffusion weighting.
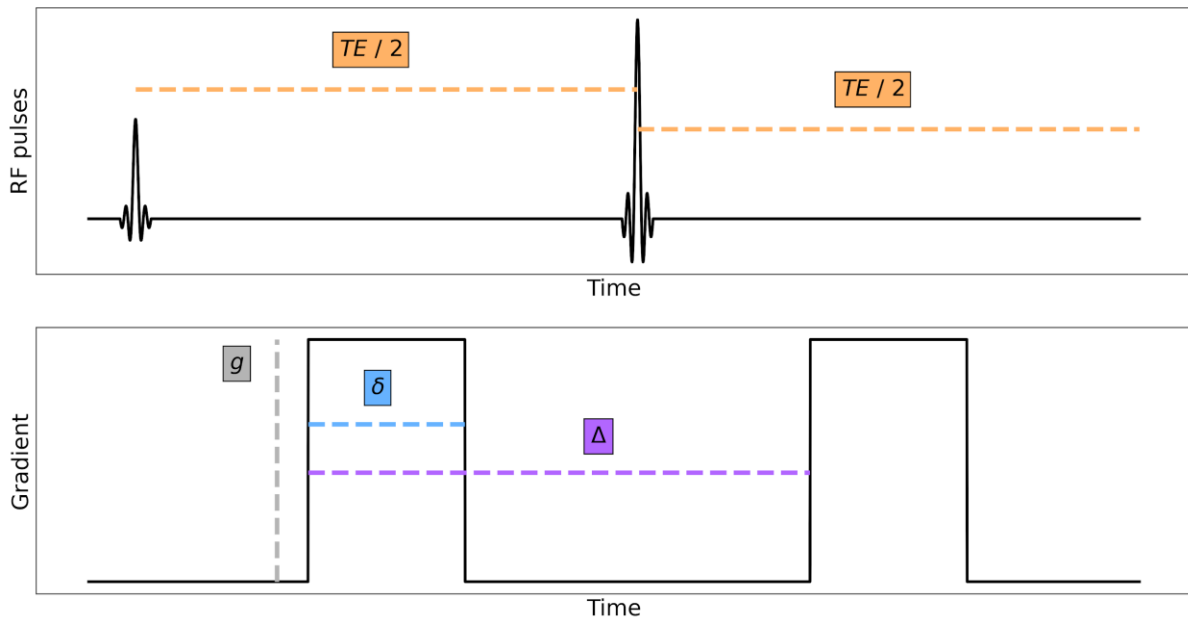
Fig. 1. Schematic representation of the PGSE experiment. In the figure, δ is the duration of each gradient lobe, Δ is the separation between the beginning of the first and second lobe, and g is the gradient strength. The term $\Delta - \delta/3$ is referred to as diffusion time. δ, Δ and g are typically combined to calculate the *b-value* ($b = \gamma^2 g^2 \delta^2 (\Delta - \delta/3)$, see Equation 4), which provides a measure of the overall diffusion weighting (the higher the value of b, the stronger the signal attenuation and the lower the signal-to-noise ratio, SNR).

The first lobe produces a spatially variant magnetic field that effectively tags the water molecule MRI phase according to their spatial position, while the second lobe is designed to cancel out such tags if the positions of the molecules do not change. In the presence of diffusion, water molecules move at random during the time interval separating the two lobes, so that the tag removal is not complete, being the final position of the molecules different from their initial one. This leads to overall dephasing when integrating the molecule phase over a spin ensemble, which results in an attenuation of the MRI signal, known as DW signal decay. More formally, let $\mathbf{G}(t)$ be the diffusion-sensitizing gradient waveform and let $\mathbf{r}(t)$ be the generic Brownian random walk overtime of a molecule. The total MRI phase accrual at the time of the

signal acquisition T for the generic molecule can be calculated as $\phi = -\gamma \int_0^T \mathbf{G}(t) \cdot \mathbf{r}(t)\, dt$,

where γ is the proton gyromagnetic ratio (equal to $267.52 \cdot 10^6$ rad s^{-1} T^{-1} for the hydrogen

nucleus ^{1}H) and $\cdot$ the dot product, while the corresponding MRI signal as $s = e^{j\phi}$. The total

MRI signal is obtained as the ensemble average of s over the spins contained in the MRI

voxel, i.e. [3]

$$A \; = < s > \; = < e^{-j\gamma \int_0^T G(t)\, \cdot r(t)\, dt} > \quad (2)$$

Notably, the typical measurement time T in real-world MRI experiments (on the order of 10-

100ms) provides water molecules sufficient time to experience the effect of the cell boundaries

at body temperature, so that the MRI signal A carries sufficient information for their

characterization. The intrinsic water diffusivity at 37 ℃ is of the order of D= 2.0 µm^2 ms^{-1}, so

that the root mean squared displacement for measurement times in the range T= 10-100ms

varies approximately in $\sqrt{<r^2>} = \sqrt{6DT} \sim$ 10-35 µm, which is comparable to the

characteristic cell sizes in most biological systems.[4]

1.3 b-value and diffusion time

Several phenomenological or biophysical models and/or representations have been

proposed to parametrize the DW MRI signal A as a function of tissue properties of interest. In

particular, two complementary approaches have been proposed for extracting information

about tissue microstructure: phenomenological signal representations from statistical

mechanics, and multi-compartment biophysical tissue models [5]. Tissue models assume a prior

picture of the underlying tissue while phenomenological representations (such as diffusion

tensor and diffusion kurtosis imaging) use rely on mathematical approximations of the DWI-

MRI signal (e.g., cumulant expansions) without assumptions about underlying tissue. Thus,

they are applicable to any tissue type, but the estimated parameters lack specificity. The

models enable the practical estimation of such tissue properties from sets of measurements

performed by varying the direction, timing, and strength of the diffusion encoding gradient $\mathbf{G}(t)$. The salient characteristics of $\mathbf{G}(t)$ are typically summarized by a parameter known as *b-value*, which provides information on the total diffusion-weighting strength.[6] The *b-value* has units of [s/m²], and is defined as

$$b = \gamma^2 \int_0^T K(t) \cdot K(t)\, dt \quad (3),$$

where $K(t) = \int_0^t G(\xi)\, d\xi$ is a function encoding the history of the diffusion encoding gradient, $\cdot$ is the dot product and T is the time at which the signal is acquired (e.g. the echo time for conventional PGSE). For the conventional PGSE diffusion experiment, expression (3) reduces to

$$b = \gamma^2\, g^2\, \delta^2\, (\Delta - \delta/3) \quad (4),$$

where δ is the duration of each gradient lobe, Δ is the separation between the beginning of the first and second lobe, and g is the gradient strength. The term $\Delta - \delta/3$ is typically referred to as *diffusion time* since it indicates the amount of time during which water molecules diffuse and senses the microstructure before the measurement is taken.

1.4 Diffusion-weighted MRI models and representations

Among the different signal models and representations proposed in the literature, diffusion tensor imaging (DTI) is certainly one of the most popular.[7] DTI provides summary information about the covariance structure of the molecule diffusion displacement distribution, which is related to the directionality of the water diffusion process. DTI offers high sensitivity to small changes at both macro- and microstructural levels in white matter (WM) tissue and is a robust technique that can be implemented under high time pressure in clinical settings in most modern scanners. Nevertheless, while DTI scalar maps emerged as a measure sensitive to tissue structure, they fail to characterize highly complex diffusion topology, as in the

presence of WM crossing fibers, where the diffusion displacement distribution is multimodal.[8] Also, despite its high sensitivity, DTI suffers from limited biological specificity concerning several microstructural tissue properties within a given voxel and is also influenced by multiple non-biological factors (e.g. scanner parameters, data quality, head motion, and so on).[9] Recently, several advanced diffusion MRI techniques have been proposed to increase the sensitivity and specificity to certain microstructural properties,[4,10] which are described in the following sections for the benefit of the readership.

2. Phenomenological signal representations

In the classical PGSE framework, the dependence of the DW signal on the diffusion encoding gradient can be handily parameterized concerning the experiment *b-value* and the gradient direction. The signal can be approximated as a function of increasing powers of b, according to a formalism known as cumulant expansion,[11,12] which is in its construction similar to the Taylor expansion of a function in the neighborhood of a point. It can be shown that the logarithm of the DW signal for a gradient direction $\mathbf{G}$ and *b-value* (b) can be written

as: $ln\ A\ =\ ln\ A_0\ +\ c_1\ b\ +\ c_2\ b^2\ +\ O(b^3)\ (5),$

where A_0 is the non-DW signal, and c_1 , c_2 , … are the coefficients of the expansion. Such coefficients can be estimated voxel-by-voxel from sets of multi *b-value* DWI (also known as *multi-shell*), and are related to the cumulants of the water molecule displacement distribution due to diffusion, also known as *diffusion propagator*.[13]

When the expansion in Equation 5 includes terms up to the first order (i.e. it discards terms proportional to b^2, b^3, etc), then the formalism is effectively equivalent to DTI. When terms up to the second-order are kept instead (i.e. terms proportional to b^3 or higher powers of b are discarded), then the formalism is equivalent to diffusion kurtosis imaging (DKI). DTI and DKI parameters are highly sensitive to the underlying microstructure, being related to the

properties of the spin displacement distribution, which carries a signature of microstructure. However, they have limited biological specificity, since they can be influenced by many factors at the same time (e.g. density of microscopic anisotropic structures, such as axons; overall geometrical configuration of such structures, as well as their intrinsic diffusion properties).

2.1 Diffusion tensor imaging

In DTI, the expansion in Equation 5 describing the logarithm of the DW signal for a gradient direction G and b includes terms up to the first order, which characterizes the Gaussian characteristics of the diffusion process. The expansion becomes as shown below:

$$ln\,A \;=\; ln\,A_0 \;-\; b\,D \quad (6),$$

where D is the apparent diffusion coefficient (ADC) along with direction G,[7] which is proportional to the variance of the spin displacement distribution and inversely proportional to the diffusion time. Practically, in standard DTI Equation 6 is generalized to 3D space introducing a *diffusion tensor* $D = [D_{ij}](i = 1,2,3; \; j = 1,2,3; \; D_{ij} = D_{ji})$, a rank-2 tensor described by a positive semidefinite matrix containing 6 independent parameters. These may be estimated with as few as six diffusion-weighted images (DWIs) with constant *b-value* non-collinear directions as well as a single non-diffusion-weighted image (b = 0) via linear or non-linear fitting. Nevertheless, the increasing number of gradient directions (~45 DWIs) can significantly improve the angular precision of the diffusion signal.[14] The fitted diffusion tensors (i.e. 3 x 3 matrices) can be mathematically decomposed in each voxel as the combination of three mutually orthogonal eigenvectors $(\epsilon_1, \epsilon_2, \epsilon_3)$ and 3 eigenvalues $(\lambda_1, \lambda_2, \lambda_3)$, with λ_i describing the ADC along spatial direction ϵ_1 for $i = 1,2,3$ and such that $\lambda_1 \geq \lambda_2 \geq \lambda_3$ such a mathematical representation of the tensor can be easily converted to a 3D geometric representation of the diffusion process, consisting of an ellipsoid with axes of length $(\lambda_1, \lambda_2, \lambda_3)$ aligned to the directions $(\epsilon_1, \epsilon_2, \epsilon_3)$. The first eigenvector ϵ_1, linked to the largest eigenvalue λ_1,

can also be used to illustrate the directionality of the tensor through a color scheme (red: the right to left or x-axis, green: anterior to posterior or y-axis, and blue: head to feet or z-axis) and the eigenvalues stored all the information on the shape and size of the tensor independently on their orientation. In regions where coherent and tightly packed bundles are present, the diffusion tensor typically takes the shape of a prolate ellipsoid ($\lambda_1 >> \lambda_2 + \lambda_3$). In regions composed of free water, such as cerebrospinal fluid (CSF), the diffusion tensor is isotropic and the equivalent ellipsoid exhibits a spherical shape ($\lambda_1 = \lambda_2 = \lambda_3$). Finally, in regions with crossing fibers, the diffusion tensor typically takes a planar shape, i.e. that of an oblate ellipsoid ($\lambda_1 = \lambda_2 >> \lambda_3$), as shown in Figure 2.
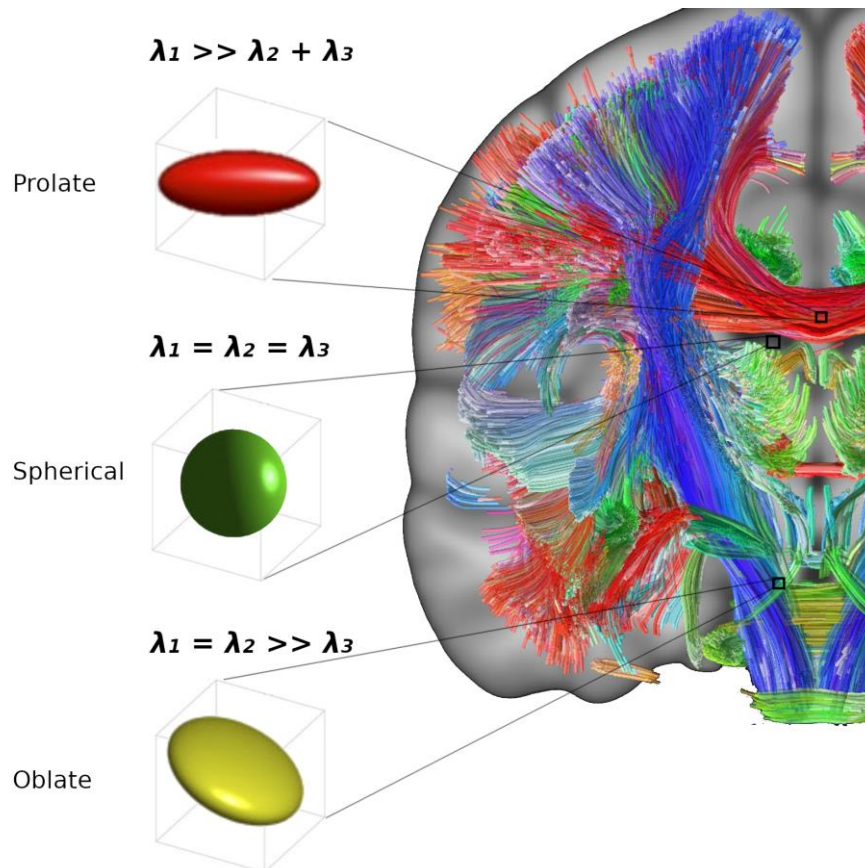

Fig. 2. An illustration in which the diffusion tensor is represented by an ellipsoid, whose principal axis in each voxel is aligned with the dominant fiber orientation.[15] In the limit case of a spherical representation, all eigenvalues are equal and the diffusion process is isotropic (i.e.

it exhibits the same characteristics along any spatial direction). Otherwise, the tensor exhibits a planar shape in crossing areas.

In DTI, several quantitative measures can be defined from the eigenvalues of the tensor.[16] The axial diffusivity (AD) is defined as the diffusion coefficient along the principal direction of the fastest diffusion of the tensor (AD = λ_1), while radial diffusivity (RD) is defined as the average diffusivity perpendicularly to the principal diffusion direction (RD = $(\lambda_2 + \lambda_3)/2$). The quantitative map that describes the average amount of diffusion in a voxel is instead obtained by averaging three eigenvalues and is known as mean diffusivity (MD = $(\lambda_1 + \lambda_2 + \lambda_3)/3$) index. Finally, fractional anisotropy (FA) describes the degree of anisotropy of the diffusion process independently of the average diffusivity and the diffusion orientation.[17] FA is a simple way of summarizing the degree of anisotropy by a range between 0 (isotropic) and 1 (anisotropic).[18] Quantitative DTI metrics are highly sensitive to changes at the microstructural level.[16] However, they are often difficult to interpret, given their limited biological specificity: several biological characteristics (e.g. myelination, axonal packing, axonal orientation dispersion) can all affect the value of each of the DTI indices. Thus, interpreting observed DTI changes is difficult in several conditions, particularly when neuropathological information is not available.[19,20] Moreover, as mentioned before in Section 1.4, one of the major limitations is the inability to disentangle the complex and heterogeneous microstructure contributions in a given voxel, such as fiber crossings.[21] Nonetheless, DTI is still widely used in scientific research due to its exquisite sensitivity to microstructural alterations beyond focal lesions, its robustness, and its quality of capturing microstructural properties in a few and interpretable parameters.

2.2 Diffusion kurtosis imaging

In DKI, the *b-value* expansion in Equation 5 includes terms up to the second-order, becoming

$$ln\, A \;=\; ln\, A_0 \;-\; b\, D \;+\; \frac{1}{6}\, b^2 D^2 K \;\;(7),$$

where D is again the ADC along with direction $\mathbf{G}$ and K the kurtosis excess along the same direction. K quantifies departures from Gaussian diffusion, such that a non-zero K (i.e. non-monoexponential decay as a function of b) can arise either in presence of multiple Gaussian compartments with different ADC (i.e. with different intrinsic D, but each with intrinsic $K = 0$), as well as in presence of barriers that restrict water diffusion.

DKI employs higher *b-values* (>2000 s/mm^2 and <3000 s/mm^2 *in vivo* in the brain) to capture information about non-monoexponential (i.e. non-Gaussian) signal behavior without making any assumptions of the underlying tissue types.[22] Indeed, the DKI may provide more sensitive and accurate measures of tissue microstructure than DTI for their ability to describe the restricted diffusion compartment within biological tissues as shown in Figure 3.[23,24] The kurtosis parameters quantify the deviation from a Gaussian distribution profile. Thus, when the diffusion behaves in a Gaussian fashion, the kurtosis coefficient approaches zeros, the signal decay is monoexponential and the diffusion properties are fully captured by simpler DTI.[12]
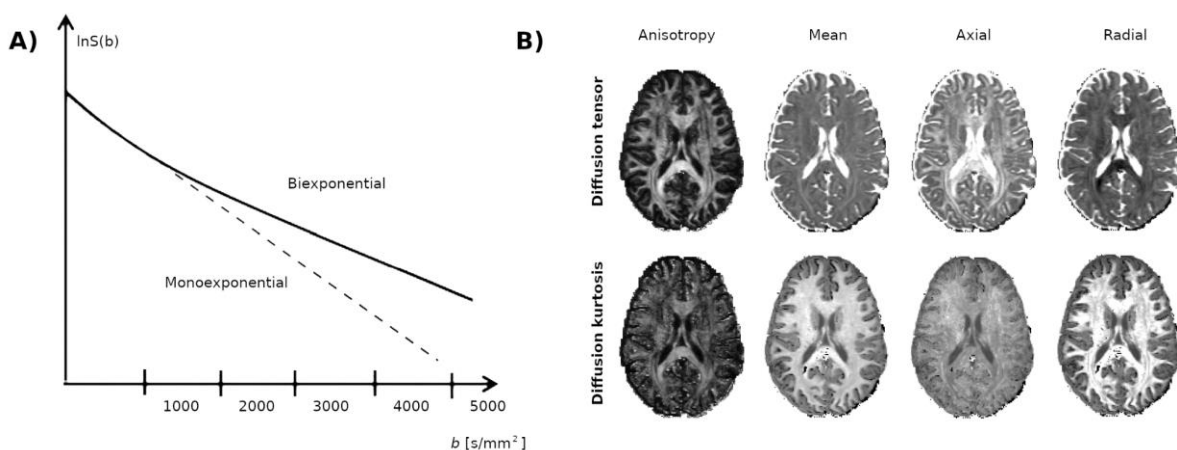

Fig. 3. Illustration of the (A) non-monoexponential MRI signal decay at higher b values (> 1000 s/mm^2) due to non-Gaussian diffusion (e.g., when imaging a two-compartment system

as in WM, leading to a bi-exponential signal decay) and (B) examples of scalar DTI and DKI maps.

In DKI, equation 7 is generalised to 3D space by introducing a rank-2 *diffusion tensor* $\mathbf{D} = [D_{ij}](i = 1,2,3; j = 1,2,3)$, with $3^2 = 9$ components and 6 independent parameters, and a rank-4 *kurtosis tensor* $\mathbf{W} = [W_{ijkl}](i = 1,2,3; j = 1,2,3; k = 1,2,3; l = 1,2,3)$, with $3^4 = 81$ components but only 15 independent parameters. The total number of parameters to estimate in each voxel in DKI is 22 (the non-DW signal level; 6 diffusion tensor parameters; 15 kurtosis tensor parameters),[22] implying that a minimal DKI protocol includes at least 21 non-collinear DW images over 2 shells, plus an additional non-DW b = 0 images. In practice, a higher number of measurements (e.g. 40 or 60) is typically used in DKI analysis, and key properties of the kurtosis tensor (i.e. axial, radial and mean kurtosis) can be computed using as few as 13 images, as shown recently in brain MRI.[25] All in all, the DKI fitting provides DTI parameters plus additional scalar metrics that provide additional information to DTI, being related to the non-Gaussian properties of the diffusion propagator.[26,27] Furthermore, DKI properties are less sensitive to certain biological confounds effects, such as regions of complex fiber architecture.[28] Although DKI is sensitive to microstructural changes in both gray (GM) and WM tissues, the DKI metrics are difficult to interpret (lack specificity) being influenced by several characteristics of the spin displacement distribution at the same time and due to other confounding effects, such as fiber orientation distribution, noise and image artifacts.[29,30]

3. Diffusion microstructure imaging

The continuous improvements in MRI scanner technology and the development of ever-faster acquisition strategies for High Angular Resolution Diffusion Imaging (HARDI) over multiple *b-value* shells have paved the way to new microstructural MRI methods aiming to increase the biological specificity of diffusion imaging, compared to DTI and DKI. As an

example, rich gradient direction schemes are mandatory to overcome some limitations of DTI, which cannot model more than one dominant orientation for each voxel.[31] In the following sections, we will first describe advanced DW-MRI techniques that enable the characterization of complex fiber configurations. Afterward, we will present several multi-compartmental models that aim to provide voxel-by-voxel estimates of key neuronal features relevant in neuroscience and neurology applications, such as axonal density. Finally, we will briefly introduce some of the latest advances in MRI acquisitions, beyond the conventional diffusion encoding based on PGSE.

3.1. Models of complex diffusion patterns in areas with multiple fiber orientations

The motivation behind the development of these models is the estimation of complex WM configurations that cannot be captured by the tensor representation. When the fibers are highly aligned in the same direction, a single tensor suffices to provide a good representation of the underlying fiber orientation. However, in presence of crossing fibers configurations, an undefined principal direction is obtained through single-tensor representations (i.e. the diffusion tensor is planar).[32] This issue can be overcome by the reconstruction of full fiber orientation distribution (FOD) functions, which provides a more complete representation of how the fibers are oriented within a voxel, see Figure 4.[33] Mathematically, the FOD is a probabilistic distribution on the sphere, which can capture distinct fiber populations contained in a voxel through distinct peaks, orientated along with different directions. HARDI acquisitions with at least 60 samples of DWIs are necessary to accurately reconstruct the FOD and resolve crossing fibers configurations.[34] The most common model-based approach to recover the FOD directly from MRI measurements is using constrained spherical deconvolution. The main idea of this method is to assume the same diffusion properties across the whole brain to characterize a unique diffusion response function of a single fiber. Then, the diffusion signal is modeled by the spherical convolution of the FOD with the estimated response function of the anisotropic shape.[35] Unfortunately, the presence of fiber crossing at shallow angles is challenging to decompose using FOD due to limited angular resolution and intrinsic FOD peak

width.[36] A recent advanced approach derived from the information of FOD amplitude has been developed to obtain more robust anatomical features in areas of crossing fibers.[37] Many quantitative scalar maps can be computed from the FOD. Among these, the apparent fiber density (AFD) holds promise as biomarkers of WM fiber integrity, as it may differentiate alterations to distinct, specific fiber bundles populations in group comparisons. Lastly, a new method proposed by Raffelt et al., has emerged to assess distinct local populations of fiber within a voxel ("fixel"). [38] The fixel-based analysis (FBA) is both sensitive and specific to resolve multiple fiber populations in areas of crossing fibers, which improves the quantitative discrimination of biological tissue patterns within a voxel compared to conventional DTI metrics. [39]
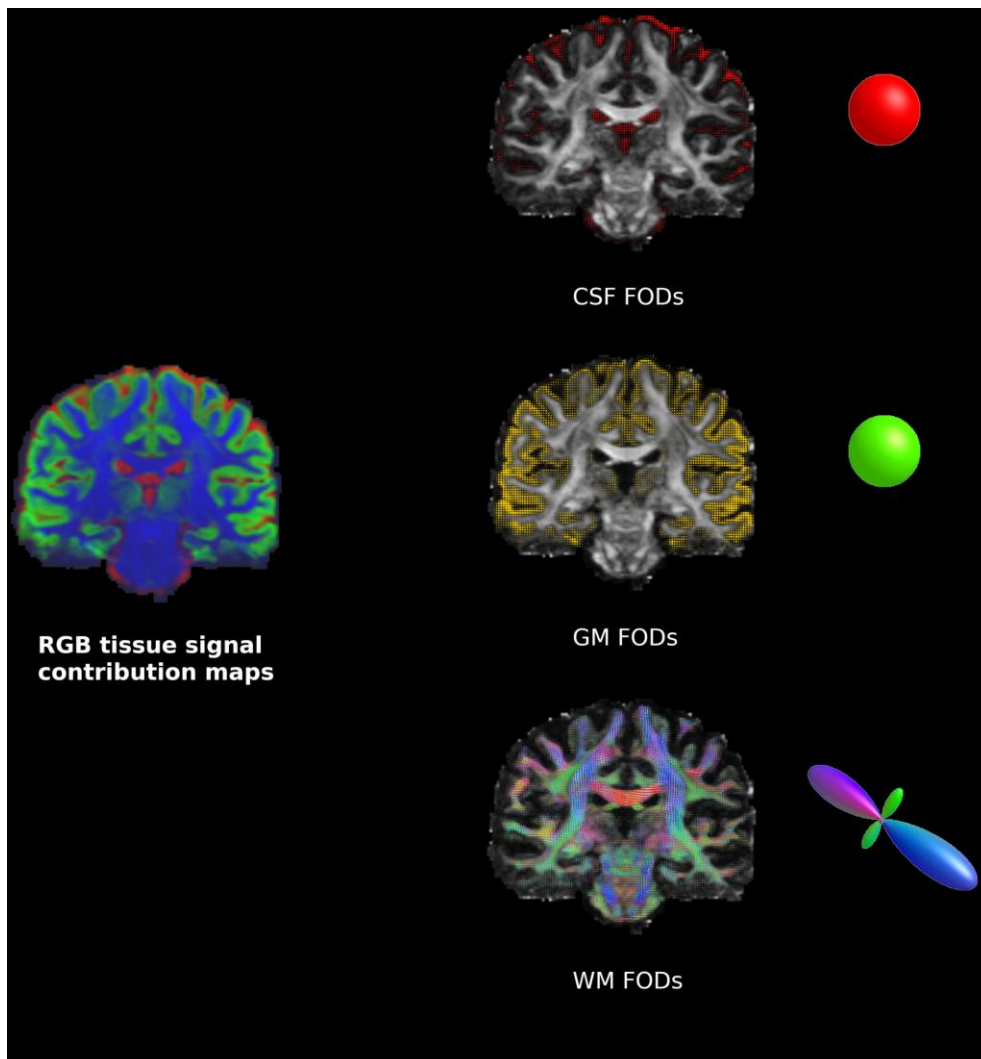
Fig. 4. The FOD reconstruction is provided by multi-shells, multi-tissue constrained spherical deconvolution (MSMT-CSD).

3.2. Biophysical tissue microstructure models

In biophysical microstructural diffusion imaging, the DW signal is modeled as the sum of the contribution of different compartments. In WM, the standard biophysical model includes two compartments,[4] modeling signals arising from intra-/extra-axonal water (excluding myelin), and can sometimes feature a third compartment to describe partial volume effects with the CSF (as shown in Figure 5). In GM, additional contributions can be included, for example, signals coming from cell bodies and neuronal somas. [40] Biophysical modeling typically requires the acquisition of both low and high b-values, sampling Gaussian and non-Gaussian diffusion behavior respectively, to resolve the properties of the compartments as well as their relative signal fractions. A variety of microstructural models have been proposed in the literature, depending on the number of compartments included in the model as well as the assumptions made to capture the salient diffusion characteristics of each compartment (i.e., model constraints). Accordingly, increasing pathological specificity is one of the main objectives of developing biophysical models in diffusion MRI research. The estimation of the microstructural properties using advanced diffusion MRI will provide novel insights for understanding the relation between brain imaging and clinical manifestations. Unfortunately, the biological validation of microstructure imaging techniques is challenging due to the changes brought by postmortem diffusion properties and scanning samples. [41] Moreover, the oversimplification of these models in comparison with the complex underlying cellular components and structures are still debated. Despite these limitations, some of the most sophisticated biophysical models can offer useful non-invasive descriptors sensitive to specific microscopic tissue features, such as axon diameter and fiber packing density. [10] We point the reader to Jelescu et al., for a detailed description of the physics and the mathematical formalism behind each microstructural model. [5] Below, we include a description of the most

promising models, making sure to point out that the appropriateness of the assumptions of each model is still a matter of debate within the diffusion MRI community. [42]
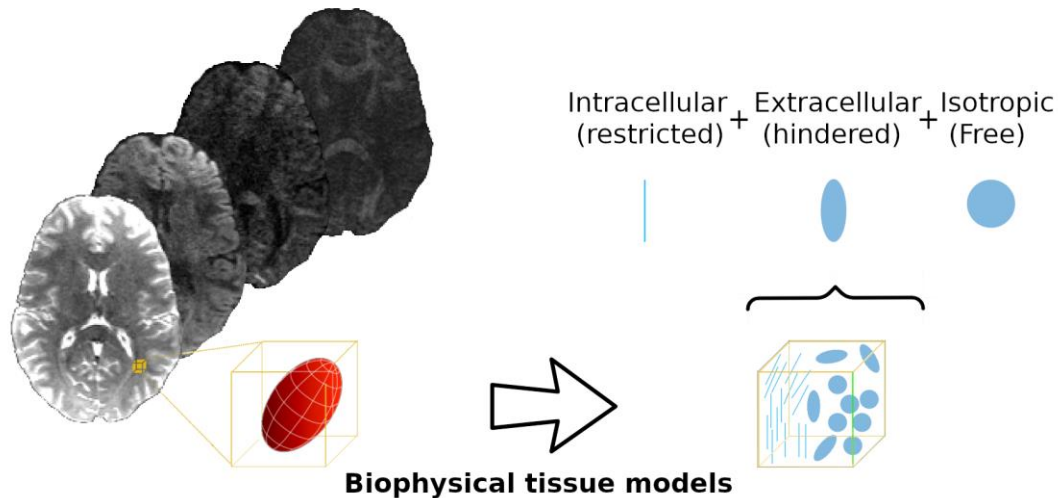

Fig. 5. An overview of biophysical tissue microstructure models. Three compartments of diffusion are shown: intra-axonal (restricted), extra-axonal (hindered) and CSF (free, isotropic water).

3.2.1. Composite hindered and restricted model of diffusion

The composite hindered and restricted model of diffusion (CHARMED) is a multi-compartment model that describes the DW signal as originating from two independent components: one, characterized by restricted diffusion and describing the intra-axonal space (non-Gaussian diffusion); the other, characterized by hindered Gaussian diffusion and describing the extracellular environment.[43] The CHARMED model adopts impermeable cylinders along multiple fiber orientations to model the restricted compartment, while the hindered compartment is described as Gaussian distribution (the dominant part of diffusion signal at low b-value). The fitted CHARMED parameters include the restricted volume fraction related to the "axonal density", the restricted fiber orientations and the apparent diffusion coefficient of the hindered compartment. To disentangle these independent populations, several assumptions are made: (1) from the acquisition point of view, the diffusion gradients

are applied perpendicularly to the fiber direction, which is therefore assumed to be known a priori (e.g., in the corpus callosum), (2) there is no orientation dispersion about the fiber direction; (3) the cylinders, modeling axons, are perfectly impermeable, and (4) all cylinders in a voxel have the same axon diameters.[44] The main drawback of CHARMED model is that, due to its increased complexity, it requires a time-demanding diffusion acquisition protocol (>3000 s/mm^2 over multiple diffusion times) to provide a robust estimate of compartmental tissue structures.[14,45]

3.2.2. Axon morphometry mapping

AxCaliber and ActiveAx frameworks are innovative diffusion methodologies that are enabled to quantify axon morphometry characteristics using sophisticated diffusion MRI acquisition methods.[46] AxCaliber is an extension of the CHARMED model that introduces an axon diameter distribution (ADD) in each voxel.[47] The intra-axonal compartment is modeled as a set of cylinders with various diameters, whose ADD follows a gamma distribution whose parameters are estimated voxel-by-voxel. To do this, AxCaliber employs a combination of different diffusion times and *b-values* with high diffusion gradient amplitude (300 mT/m) to measure the diffusion properties exactly perpendicular to the fiber orientation.[48] The previous implementation of AxCaliber in vivo data has demonstrated the feasibility of the axon diameter measures on rat corpus callosum on five established regions when it has been compared with the same sample by histological analysis.[49] However, later work has suggested that AxCaliber may overestimate the ADD quantification within a voxel because it does not account for axonal orientation dispersion.[50]

To overcome both limitations, a suitable scan time for "in vivo" human imaging enabling the estimation of both axon diameter and density, the ActiveAx technique was proposed.[51] The ActiveAx model describes the diffusion signal as a contribution of the restricted (within cylinders, modeling axons), hindered (in the extra-axonal space, including cell bodies) and isotropic (i.e. in partial volume with CSF) diffusion compartments. This model is capable to estimate the intra/extra-axonal volume fractions and the axon diameter index with a large

volume of high-quality DWI data. Several assumptions have been made in the ActiveAx model fitting to obtain the axon morphometry indices, namely: an equal value of intrinsic diffusivity of intra-axonal water and parallel diffusivity of the hindered compartment and the absence of axonal dispersion effects (all bundles are considered to be aligned axons with identical radii and orientation). The axon diameter indices obtained by ActiveAx using ultra-high gradient strengths acquisitions are comparable to the histological imaging measures, however, the results achieved through PGSE acquisition protocol using lower gradient strength are not sensitive to small diameters of axons.[52]

3.2.3. White matter tract integrity

The biophysical white matter tract integrity (WMTI) model assumes highly coherent WM bundles and neglects the CSF compartment. WMTI links a two-compartment biophysical model of neural tissue, accounting for intra-/extra-axonal water, to the *b-value* expansion of the DW signal up to the power of b^2, i.e. to DKI metrics.[53] In practice, in WMTI the intra-/extra-axonal parallel diffusivities and intra-axonal volume fraction are computed analytically from the apparent diffusion and kurtosis tensors. These can be typically estimated via linear least squares, avoiding the need for time-consuming non-linear fitting of multi-exponential models. More recent approaches, such as LEMONADE,[54] follow a similar approach in that they estimate tissue parameters analytically given the coefficients of *b-value* expansions but considering higher-order expansions (i.e. beyond b^2). In general, approaches such as WMTI or LEMONADE enable the computation of biophysical tissue parameters with limited fitting constraints. However, they are often difficult to implement in clinical settings, since they require very long acquisition times to enable the estimation of high-order tensors, which are notoriously noisy and prone to measurement errors. According to previous studies,[55,56,57] the WMTI metrics, axonal water fraction and diffusion hindered tortuosity, showed a capability to distinguish specific mechanisms on the tissue damage and disability progression.

3.2.4. Neurite Orientation Dispersion and Density Imaging

Neurite orientation dispersion and density imaging (NODDI) has recently been proposed for clinically feasible mapping of neurite morphology over the whole brain.[58] Neurites include axons in WM and axons/dendrites in GM. The NODDI technique uses a three-compartment tissue model to describe multi-shell DW acquisitions. The intra-neurite space is modeled by a collection of "sticks" (i.e. zero radius cylinders), oriented according to a Watson/Bingham distribution defined over the sphere the extra-neurite space (including cell bodies) is described as a cylindrically symmetric diffusion tensor (hindered Gaussian diffusion, i.e. similarly to DTI when $\lambda_2 = \lambda_3$); the free water compartment is described as an isotropic diffusion tensor with intrinsic diffusivity of 3 μm^2/ms. Both intra-/extra-neurite compartments have the same intrinsic diffusivity, which in *in vivo* imaging is not estimated from the data but is fixed across the whole brain to 1.7 μm^2/ms. Moreover, the perpendicular diffusivity of the extra-neurite compartment is calculated analytically by combining the extra-neurite volume fraction and parallel diffusivity in a tortuosity model.[59] Fitting the NODDI model voxel-by-voxel provides maps quantifying the degree of orientation coherence or neurites, as well as their density. The first feature is characterized by the orientation dispersion index (ODI), while the second one by the intra-neurite volume fraction, also known as neurite density index (NDI, sometimes also referred to as intra-neurite volume fraction or intra-cellular volume fraction, ICVF). Finally, the isotropic volume fraction (isoVF) quantifies the local amount of partial volume with free water (e.g. with CSF of edema in inflammation). Both ODI and NDI range from 0 to 1. An ODI of 0 implies that neurites are all perfectly aligned among each other, while an ODI of 1 implies that they are completely dispersed in space (i.e. randomly distributed). On the other hand, increasing NDI and isoVF respectively imply increasing local density of neurites and free water. One of the main advantages of the NODDI model is the clinical feasibility acquisition, with a minimum requirement of two-shell HARDI data, which are needed to fit the model robustly in both GM and WM tissue. NODDI parameters have been demonstrated to be more specific metrics of tissue damage than DTI-derived indices and

provided significant correlations with a variety of histopathological processes in multiple sclerosis (MS).[60] Importantly, the NODDI model makes some strong assumptions on tissue microstructure that are not guaranteed to hold across the whole brain and, above all, in pathology. For example, recent works have demonstrated that fixing the value of the neural diffusivity to 1.7 μm^2/ms to the whole brain and adopting a tortuosity model for the extra-neurite, perpendicular diffusivity may produce biased parametric maps that are misrepresenting the real underlying microstructural changes.[61,62] Moreover, it has also been shown that NODDI metrics, for example NDI, are less reliable in GM than in WM, suggesting that the assumptions beyond the NODDI geometric model are better suited to capture the salient microstructural characteristics of WM, than GM.[63]

3.2.5. Spherical mean technique

The spherical mean paradigm relies on the fact that the spherical mean of the DW signal (i.e. its average over sufficient, isotropically-distributed diffusion directions at fixed diffusion-encoding strength/diffusion time) is independent of the underlying FOD, but relies on the intrinsic characteristics of the single fiber element.[64] This observation is used in the multi-compartment spherical mean technique (MC-SMT) to fit the parameters of a two-compartment model,[65] including an intra-/extra-neurite compartment as shown in Figure 6 (i.e. similar to NODDI, but without free water), without imposing any specific form to the FOD (e.g., like a Watson distribution in NODDI). To reduce the number of parameters estimated from the DW signal under the same mathematical framework, the MC-SMT model makes certain assumptions on the biophysical properties of the diffusion in the tissue, i.e.: (1) the intra-neurite radial diffusivity is assumed to be zero, (2) the AD in intra-/extra-neurite compartments are equal and (3) the transverse extra-neurite diffusivity signal is defined as tortuosity model.[59] MC-SMT provides the voxel-wise maps of NDI, intrinsic neural diffusivity and orientation dispersion entropy (ODE). The ODE measures how different the ODE is from a uniform distribution, and conveys similar information to NODDI ODI but with reversed contrast (increasing ODE implies decreasing neurite orientation variability). Kaden et al., studied a

tuberous sclerosis mouse model that demonstrated a direct link between microscopic diffusion indices and the quantification of myelin and axonal loss compared to controls.[65] Although MC-SMT does not make any assumptions about the orientation distribution and estimates the neural diffusivity from the data (unlike NODDI), the intra-voxel microscopic heterogeneity may bias MC-SMT metrics.[66] A recent study has shown that metrics from NODDI and MC-SMT show similar correlations with conventional DTI indies and detect microstructural alterations due to multiple sclerosis that go in the same direction.[67]
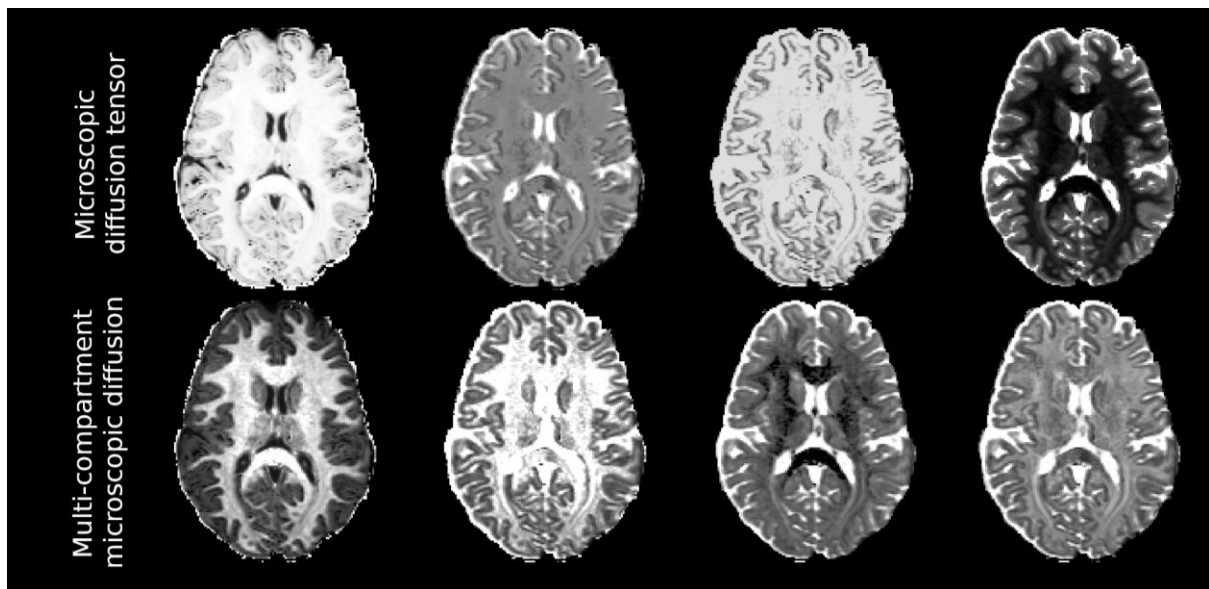

Fig. 6. Examples of microstructural parameter maps provided by the MC-SMT framework (top: fitting of a single-compartment model to spherical mean signals, providing the intrinsic properties of the diffusion tensor characterizing a fiber bundle; bottom: fitting of a two-compartment model to spherical mean signals, providing estimates of the intra-/extra-neurite properties in a fiber bundle), which are not confounded (i.e. they are independent) of the underlying FOD.

3.2.6. Diffusion Basis Spectrum Imaging

The diffusion basis spectrum imaging (DBSI) multi-tensor approach was proposed as a linear combination of multiple anisotropic and isotropic diffusion tensors to describe the full range of intra-voxel heterogeneities in diffusivities.[68] The DBSI model assumes no exchange between intra-/extra-axonal compartments, and the isotropic diffusion patterns are separated from the other compartments to discriminate between diffusion within highly cellular tissue, vasogenic edema and non-restricted water diffusivity within CSF.[69] DBSI is capable to generate distinct DBSI quantitative parameter maps that represent the anisotropic tensor (apparent axonal density), the restricted diffusivity (apparent cellularity) and the free isotropic diffusivity (CSF). DBSI holds promise to disentangle concurring axonal injury, demyelination and inflammation.[69,70] However, DBSI requires the acquisition of a high number of DW measurements to accurately separate the different diffusion regimes within a voxel, and as a consequence may not be feasible in most clinical settings, where scan time is limited.

3.3. Hybrid models

The hybrid models characterize the diffusion signals by combining multi-compartment biophysical modeling and signal representations (e.g., DTI and DKI).

3.3.1. Free Water Elimination

The two-tensor free water elimination (FWE) technique was developed to separate the isotropic free water component from the rest of the microstructural tissue properties, aiming to increase the sensitivity and specificity of the diffusion measures both in health and pathological conditions.[71] In FWE, the total DW signal in a voxel is modeled as the combination of a neural tissue compartment, characterized by a single diffusion tensor, as in DTI, and by an isotropic diffusion compartment, aiming to capture CSF partial volume. Such a free diffusion component was also associated with other pathological processes in neurodegenerative disorders, such as Alzheimer's disease (AD) or schizophrenia.[72,73] One of the major advantages of the FWE model is that it does not require spatial constraints or assumptions to be estimated and their clinical feasibility.[74] Additionally, the FWE model is capable of measuring DTI indices without

the effects of CSF partial volume effects to improve the reliability of these metrics and the test-retest reproducibility.[75]

3.3.2. Distribution of anisotropic microstructural environments in diffusion imaging

The distribution of 3D anisotropic microstructural environments in diffusion-compartment imaging (DIAMOND) has been recently proposed by Scherrer et al. [76] The DIAMOND model decomposes the intra-voxel tissue compartments by a mixture of continuous distributions of diffusion tensors to capture the whole microstructural properties at a sub-voxel resolution, [77] similarly to DBSI. DIAMOND aims to better capture the multidimensional characteristics of intra-voxel diffusivity, as well as tissue heterogeneity within complex microstructural environments. Both intra-/extra-axonal diffusion by a single and symmetric distribution of 3D diffusivities. [78] To accomplish this, DIAMOND requires numerous *b-values* with uniform angular coverage and low TE, which are likely to be unfeasible to acquire in most clinical settings.

Table 1 summarizes the main features of the brain microstructure diffusion models. Note that the terms axonal density, neurite density index, (intra-)axonal water fraction, intra-

neurite volume fraction are used interchangeably in literature to indicate the fraction of the

restricted water compartment in white matter modelling axons.

	Models	Assumptions	Main quantitative maps
Signal Representations methods	DTI	Acquisition comprising at least one non-zero b-values at fixed diffusion time, with b-value not exceeding roughly 1000-1500 s/mm^2 in the brain	Diffusion tensor elements, sensitive to changes of both macro- and microstructural tissue structure
	DKI	Acquisition comprising at least two non-zero b-values at fixed diffusion time, with b-values not exceeding roughly 2500-3000 s/mm^2 in the brain	Diffusion tensor and diffusion kurtosis elements, highly sensitive to multiple factors of microstructural properties
Biophysical multi-compartment models	CHARMED	Two non-exchanging compartments (restricted and hindered diffusion), modelling intra-/extra-axonal space, with restricted diffusion assumed to take place within impermeable cylinders with the same axon diameters; multiple fibre populations per voxels; intra-axonal perpendicular diffusivity and axon diameter fixed to literature values before fitting. Rich multi-shell data acquisition at fixed diffusion time required.	Axonal density, extra-axonal diffusion tensor
	AxCaliber	Two non-exchanging compartments (restricted and hindered diffusion), modelling intra-/extra-axonal space, with rRestricted diffusion assumed to take place within impermeable cylinders with gamma-distributed diameters; multiple fibre populations per voxels. Rich multi-shell, multi-diffusion time data acquisition required.	Axon diameter; axonal density
	ActiveAx	Three non-exchanging compartments (intra-/extra-neurite; isotropic; an additional stationary water compartment required for fixed tissue); Single diameter index (identical radii and orientation); intra-/extra-neurite intrinsic diffusivities equal to 1.7µm^2/ms; free water diffusivity equal to 3.0µm^2/ms; tortuosity constraint for extra-axonal perpendicular diffusivity; no modelling of orientation dispersion variability	

	WMTI	Two non-exchanging compartments (intra-/extra-axonal); coherently aligned axons (model applicable only in areas featuring one, coherent fibre population, e.g., the corpus callosum); the model can be fitted to a DKI-like data set	Axonal water fraction; intra- and extra-axonal diffusivities
	NODDI	Three non-exchanging compartments (intra-/extra-neurite; isotropic); zero intra-neurite perpendicular diffusivity; intra-/extra-neurite intrinsic diffusivities equal to $1.7 \mu m^2/ms$; free water diffusivity equal to $3.0 \mu m^2/ms$; tortuosity constraint for extra-axonal perpendicular diffusivity; neurite orientations distributed according to a Watson/Bringham distribution. The acquisition must include b = 0 images plus two non-zero b-value (one of approx. 1000 s/mm^2 and one of approx. 3000 s/mm^2)	Orientation dispersion index, neurite density (i.e., intra-neurite volume fraction) index and isotropic volume fraction
	MC-SMT	Two non-exchanging compartments (intra-/extra-neurite); zero intra-neurite perpendicular diffusivity; intra-/extra-neurite intrinsic diffusivities are equal; tortuosity constraint for extra-axonal perpendicular diffusivity. The acquisition must include b = 0 images plus two non-zero b-value (one of approx. 1000 s/mm^2 and one of approx. 3000 s/mm^2)	Orientation dispersion entropy, neurite density index (i.e., intra-neurite volume fraction), intrinsic neural diffusivity
	DBSI	Multi-compartment model with one anisotropic compartment per fibre population; multiple isotropic diffusion compartments. No water exchange among compartments; threshold of 0.3 $\mu m^2/ms$ used to distinguish between restricted and hindered isotropic diffusion. Rich multi-shell acquisition protocol including roughly 100 images	Intra-axonal water fraction; restricted isotropic water fraction (mapping cellularity); hindered isotropic water fraction (mapping vasogenic oedema)

4. Advanced diffusion encodings

Over the last decade, advanced diffusion sequences are gaining popularity in diffusion imaging. The use of these advanced acquisition strategies provides a powerful tool to improve the specificity of the quantitative measures related to the tissue microstructure.[4] However, the advanced data acquisition techniques on 3T clinical scanner require further research before its clinical application, and the availability of such novel acquisition approaches in vendor-provided exams remains limited.

4.1. Oscillation gradient spin echo

Oscillating diffusion encoding (ODEnc) sequences use oscillating gradient waveforms over multiple frequencies to probe very short diffusion times (~ 1ms) along a single direction, as shown in Figure 7. This provides better tissue contrasts and smaller length scales and increases the sensitivity of the acquisition to the intrinsic diffusivity of the tissue (i.e. with the limited effect of restriction caused by cell membranes).[79,80] Moreover, for the case when gradients are not exactly perpendicular to neural fibers (as in presence of orientation dispersion), ODEnc enables better angular resolution at a lower *b-value* compared to standard PGSE acquisition.[81] This is particularly advantageous on the high-performance gradient amplitude (300 mT/m), where ODEnc sequences provide better sensitivity to restricted diffusivity effects increasing the reliability of the microstructural feature measurement.[82]

4.2. Double diffusion encoding

Differently from the conventional PGSE acquisition, the double diffusion encoding (DDE) advanced protocol combines two successive diffusion encodings gradients separated by a mixing time before the signal readout, see Figure 7.[83] DDE is typically performed by varying the angle between the pairs of diffusion encodings with a specific mixing time. This enables resolving microstructural properties (size and shape) as well as diffusion displacement correlation tensors within a voxel.[84,85]

4.3. B-Tensor encoding

The B-tensor encoding was developed to remove the effects of tissue orientation and improve the sensitivity of specific microstructural properties.[63] This type of sequence replaces the pulsed-gradient encoding paradigm with diffusion-encoding waveforms design (Figure 7).[86] Other benefits included in the gradient waveform is their ability to minimize the common effects of diffusion-encoding gradients, such as eddy currents.[87] The B-tensor encoding gives access to new diffusion contrasts that are not achievable with linearly polarised diffusion gradients, as in PGSE.[88] This enables disentangling cytoarchitectural scenarios that would provide the same PGSE signal, as a distribution of isotropically restricted compartments with various radii from the distribution of randomly-oriented anisotropic compartments. This holds promise in several applications, for example in brain tumors.[89]
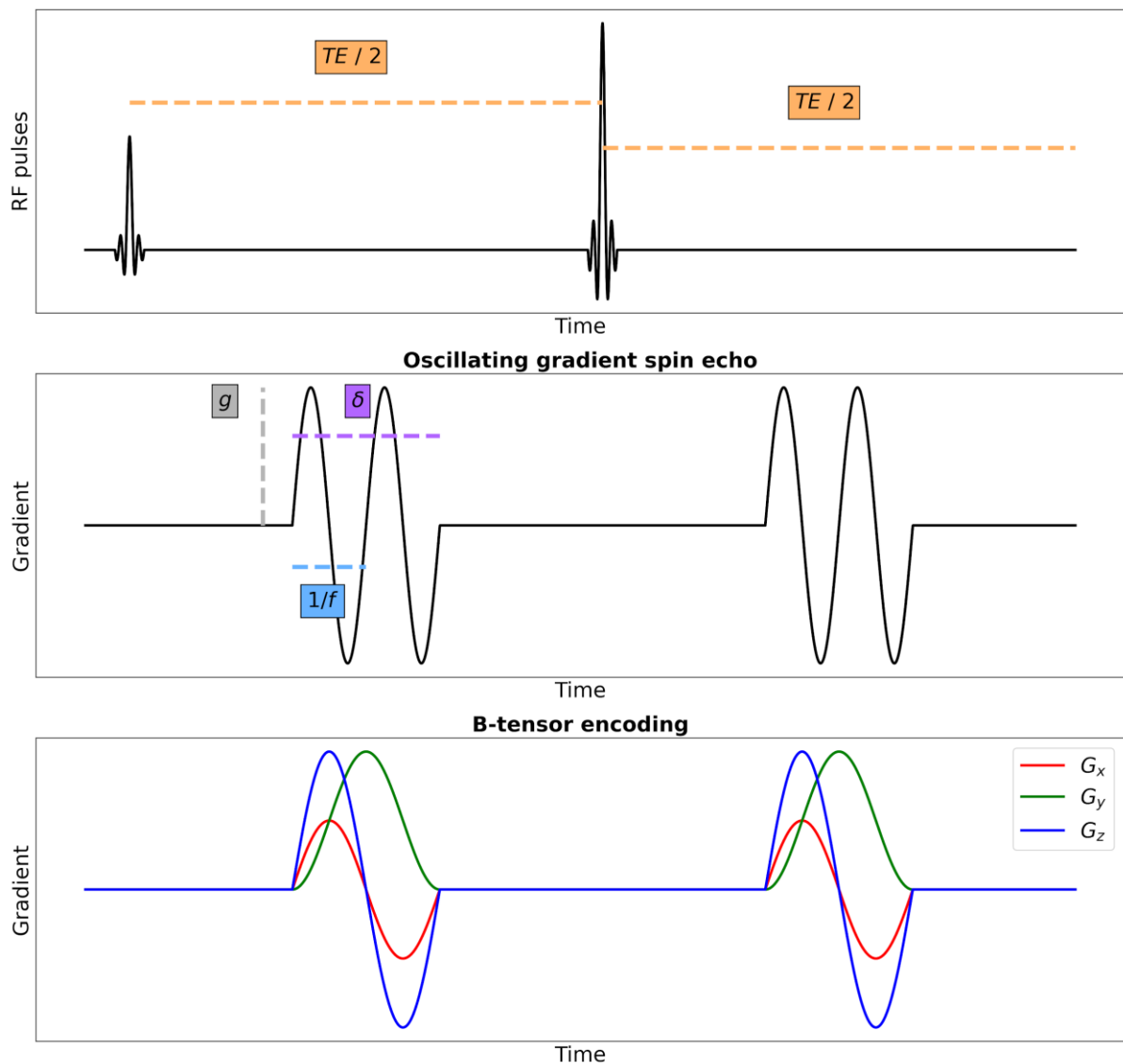
Fig. 7. Schematic representation of the OGSE and b-tensor encoding experiment. In OGSE, the gradient lobes on either side of the spin-echo refocusing pulse are not pulsed as in PGSE, but exhibit an oscillating waveform. However, the gradient is still linearly polarised, in that its direction does not change over time, hence that the three independent components of the gradient vector (x, y and z) are perfectly in phase. The *b-value* is proportional to the cube of the oscillation duration δ (i.e. to δ^3), while the diffusion time is proportional to the oscillation period $1/f$. In the b-tensor encoding instead, the diffusion gradient is not necessarily linearly polarised (e.g., it can feature spherical polarisation, planar polarization, etc), leading to unique waveforms for each of its x, y and z components.

5. Clinical applications

Diffusion studies have been widely used to analyze cerebral microstructural changes in patients with several neurological diseases.[90] Results have demonstrated abnormal tissue microstructure with subsequent loss of structural network integrity.[91] However, DTI does not account for structural heterogeneity and is affected by multiple confounding tissue properties leading to reduced specificity of clinically relevant pathological features. Advanced multicompartmental diffusion methods can characterize the diffusion signal in the presence of multiple tissue compartments and increase the specificity for tissue subtypes and the associated damage.[92,93] Therefore, they may be more suitable tools to describe disease burden in pathologies of the central nervous system and be considered as new biomarkers of demyelination and neurodegeneration, which can be used to unravel disease progression before irreversible disability manifests.[93] Some of those methods have recently been applied in several clinical conditions such as traumatic brain injury,[94] brain tumors[95] and neurodegenerative diseases.[96]

5.1. Multiple sclerosis

MS is an immune-mediated, demyelinated and neurodegenerative disease of the central nervous system characterized by focal lesions and diffuse damage involving demyelination, neuroaxonal damage and gliosis, which leads to significant clinical variability among patients.[97] DTI-derived measures, mainly FA and MD, have been extensively used to grade the severity of damage inside lesions and in normal-appearing WM (NAWM),[98] found from early stages of the disease. Decreased FA and increased MD seem to be more pronounced in advanced stages and are partially linked with physical and cognitive disability.[99] However, inconsistent results have been found in the study of GM with some reports describing decreased or increased FA values, this latter possibly due to tissue compaction.[100] Multicompartmental diffusion models have been demonstrated to be more accurate and

provide more precise microstructural tissue information.[60,101] Patients with MS showed decreased mean kurtosis (MK), one of the parameters derived from DKI, that has been associated with lower axonal and myelin density in NAWM and normal-appearing GM in both the brain and spinal cord.[102,103] DKI metrics correlated with physical disability assessed by the Expanded Disability Status Scale (EDSS).[104] Studies using NODDI reported a reduction in the NDI in lesions compared to NAWM in the brain and spinal cord of patients with MS compared with healthy controls.[60,105,106] Reduced NDI has also been observed in GM.[103] Lower NDI was associated with higher lesion load, greater physical disability assessed by EDSS but not with cognitive behavior.[105] On the contrary, ODI changes that may reflect reduced angular variations of axons possibly caused by demyelination were more contradictory. Authors found both reduced or increased ODI in lesions compared to normal-appearing tissue.[105,106] Inconsistencies may be due to degrees of axonal loss and tissue inflammation.[105–107] Moreover, the reduction of corpus callosum neuronal density, measured by NDI, is associated with lower neuronal density in WM lesions and suggests retrograde neurodegeneration of axons transected from the WM damaged.[105–107] Axonal volume fraction and intrinsic diffusivity measures of MC-SMT have demonstrated the potential to differentiate tissue subtypes in the brain and spinal cord of patients with MS,[93,108,109] and combined with DTI, indices improve the definition of the amount of damage within MS lesions,[110] see Figure 8. Overall, results demonstrate that more sophisticated microstructural measures are more sensitive than DTI indices, they can provide us with additional information on brain damage, and therefore, be more accurate and powerful biomarkers of tissue disease burden in MS patients compared with DTI.[60,103,111] However, further efforts are needed to translate the results into clinical practice.
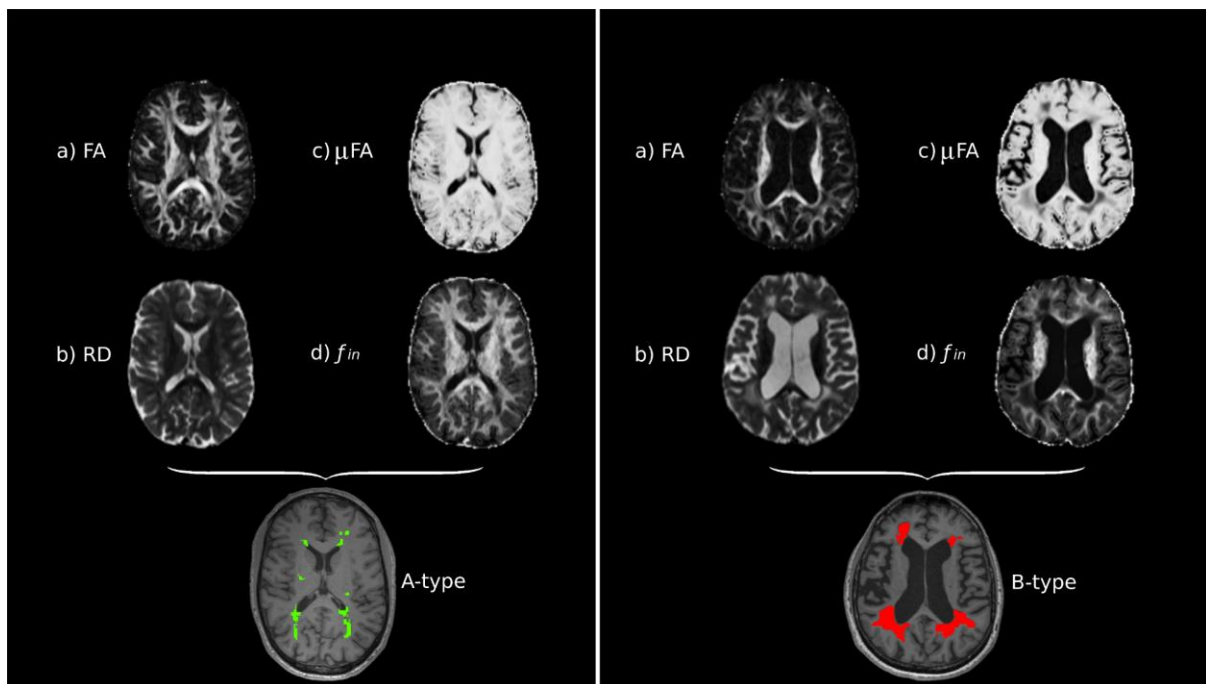
Fig. 8. MS lesions characterisation based on diffusion properties. The diffusion maps from the DTI (a, b) and MC-SMT models (c, d) are able to reflect different degrees of damage into MS lesions types. Regardless of the lesion location, B-type had larger diffusion changes (lower FA, μFA and f_{in}, yet a higher RD) and higher volume compared to the type-A lesions. The number and volume of B-type lesions were associated with disease severity and clinical and cognitive decline [110]. FA = fractional anisotropy; RD = radial diffusivity; μFA = microscopic fractional anisotropy; $f$in = intra-neurite volume fraction.

5.2. Stroke

Stroke is a major cause of death worldwide. Neuronal death in the brain area affected by ischemia is accompanied and sustained by inflammation, edema, and tissue remodeling. Those events eventually lead to axonal degeneration of connected brain regions through Wallerian degeneration. Neuroimaging is essential for stroke assessment and although computed tomography is the most used neuroimaging technique due to its wider availability in the acute phase, DWI is considered the most sensitive technique to depict infarct. Indeed, ADC reduced values are considered to demonstrate the presence of cytotoxic (intracellular)

edema, a sign of irreversible lesion, and represent the best image marker for the infarct core.[112] Advanced diffusion techniques have been applied to characterize microstructural changes in brain tissues during ischemic stroke and its sensitivity has been compared with DTI and DKI. NODDI showed increased NDI and ODI and lower isoVF in lesions compared to contralateral areas. Changes in NODDI metrics were larger than those found with other techniques, supporting a larger sensitivity to damage. Moreover, isoVF was correlated with the duration since stroke onset and was different among the distinct periods of ischemic stroke, indicating an added value to characterize the lesion stage.[113] Other studies investigating changes between subacute and chronic phases of a stroke found a significant FA and AD reduction in the ipsilateral posterior limb of the internal capsule and the cerebral peduncle compared to the contralateral one, a significant decrease in kurtosis anisotropy (KA) and higher ODI without significant alterations in Fic (intra-neurite volume), suggesting that in subacute phase fiber dispersion is the main alteration. In chronic phases, Fic reduced significantly, potentially due to a reduction in the fiber volume in parallel to disorganization of fibers indicated by persistent higher ODI values in the ipsilesional hemisphere, which could be compatible with Wallerian degeneration.[114] ODI results have also been associated with clinical outcomes. [115] Recently, single-Shell 3-Tissue Constrained Spherical Deconvolution (SS3T-CSD) was applied to differentiate within different classes of WM hyperintensities (WMHs) in patients with previous ischaemic stroke. The authors found that juxtaventricular and periventricular WMHs exhibited a relatively greater fluid-like (free water) content compatible with the accumulation of interstitial fluid compared to deep WMHs. Thus, the technique provided evidence of the heterogeneity of those lesions in vivo.[116]

5.3. Alzheimer disease

AD is the most common neurodegenerative disorder characterized by gradual memory deficits. The underlying pathological changes of AD involve the accumulation of amyloid-β (Aβ) and hyperphosphorylation of tau protein, both of which lead to the formation of Aβ plaques and intracellular neurofibrillary tangles, resulting in neuronal death.[96,117] Diffusion MRI, most

using DTI measures, has been widely applied to the study of WM and GM damage in patients with AD. Results showed reduced FA and increased MD in the core areas of the disease, including the corpus callosum, temporal lobes, cingulate gyrus, precuneus and frontal pole. DTI is also sensitive in detecting diffusion changes in patients with mild cognitive impairment (MCI), considered an early stage of AD, being more pronounced with disease severity.[96,117,118] However, DTI measures are not more informative than temporal structural volumetric in the early stages of the disease.[96] Diffusion kurtosis studies demonstrated the superiority of the DKI measures in detecting early microstructural changes both in MCI and in AD compared to healthy controls, as well as, during the trajectory of the disease course.[96,119] Changes were mainly observed in the temporal and frontal poles and the corpus callosum of patients with both AD and MCI compared to healthy controls, with the lowest values observed in patients with AD. Although DKI is superior in detecting WM abnormalities to DTI measures, the combination of both techniques significantly improves the automatic tissue discriminating task.[120] Using the NODDI technique, a reduced widespread neurite dispersion was evidenced in both cortical GM and WM microstructural tissue in patients with AD, especially in areas described as relevant for the disease.[117,118] Studies described that patients displayed lower NDI values and ODI than healthy controls in the medial and inferior temporal cortex and precuneus adjusted for cortical thickness,[118] and in the corpus callosum superior longitudinal fasciculus and WM of the frontal and occipital lobes.[117] Lower NDI was also observed in the precentral cortex, an area partially preserved from atrophy in patients suggesting that the microstructural changes may precede volume reduction.[118,121] NODDI metrics were associated with cognition.[117,122] Additionally, apolipoprotein (APOE) ε4-positive carriers, a genetic risk factor for heritable AD, displayed widespread NDI reductions in the parieto-occipital lobes while ε4-negative carriers showed more focal posterior reductions suggesting different patterns of WM damage in patients.[122]

5.4. Tumors

Gliomas and brain metastasis are the most common intracranial neoplasms. Indeed, differential diagnosis and glioma grading are essential to determine the prognosis and clinical management. DKI has been applied to distinguish gliomas from other intra-axial brain tumors in several studies and a systematic review and meta-analysis have shown an estimated sensitivity of 0.87 in the differentiation between high and low-grade glioma from the 2016 World Health Organization glioma classification.[123] These results indicate that MK has good diagnostic accuracy and seems to be a useful index of tissue complexity.[123,124] However, there is only scarce information on its ability to differentiate gliomas from other brain tumors.[123] DKI has been compared with DTI in discriminating high-grade glioma recurrence from pseudoprogression, and while relative MK and relative MD were significantly different between enhancing lesions or perilesional edema in high-grade glioma compared to pseudoprogression, relative MK appeared to be the best independent predictor.[125] NODDI has also been recently applied to the assessment of glioma grades, delineate tumoral and peritumoral areas and differentiate between glioblastoma and solitary brain metastasis. ODI and NDI were different between WHO glioma grades,[126] with the high predictive power of intracellular volume for glioma grading.[127] Also, NDI had the best distinguishing power comparing fibers inside normal, tumoral and edematous regions.[128] Extracellular volume had an area under the receiver operating characteristic curve of 0.87 for differentiating between glioblastoma and metastasis.[95] Finally, when comparing different diffusion-weighted MRI models, isoVF from NODDI outperformed other techniques in differentiating high-grade gliomas from metastases.[95,129]

6. Conclusions

In conclusion, diffusion-weighted imaging offers unique opportunities to characterize neural tissue microstructure *in vivo* non-invasively through a variety of techniques that focus on different aspects of the diffusion contrast. Elegant, phenomenological approaches such as DTI or DKI offer great sensitivity to microscopic alterations but provide metrics that are

influenced by several neuropathological characteristics at the same time. Conversely, multi-compartment biophysical models aim to improve diffusion imaging's pathophysiological specificity compared to DTI and DKI. Nonetheless, they often require making several assumptions and/or oversimplifications on the underlying neural tissue characteristics to keep model computation feasible even with short, clinical protocols, implying that their metrics must be interpreted with care, especially in disease. The next generation of quantitative diffusion imaging, based on new diffusion encoding strategies such as b-tensor encoding, holds promise as a versatile tool that better captures salient tissue microstructural features in both healthy and pathological conditions, and is therefore likely to play a key role in the clinical translation of MRI research to clinical practice.

REFERENCES

1. A. Einstein: The collected papers of Albert Einstein, 1987

2. J.E. Tanner: Use of a Pulsed Magnetic-field Gradient for Measurements of Self-diffusion by Spin-Echo Nuclear Magnetic Resonance with Applications to Restricted Diffusion in Several Tissues and Emulsions, 1966

3. E. Fieremans, H.-H. Lee: Physical and numerical phantoms for the validation of brain microstructural MRI: A cookbook. Neuroimage 182:39–61, 2018

4. D.S. Novikov, E. Fieremans, S.N. Jespersen, et al: Quantifying brain microstructure with diffusion MRI: Theory and parameter estimation. NMR Biomed 32:e3998, 2019

5. I.O. Jelescu, M.D. Budde: Design and validation of diffusion MRI models of white matter. Front Phys 28, 2017

6. Quantitative MRI of the brain : principles of physical measurement: Principles of Physical Measurement, Second edition, 2nd ed., CRC Press, Boca Raton, FL, 2018

7. P.J. Basser, J. Mattiello, D. LeBihan: MR diffusion tensor spectroscopy and imaging. Biophys J 66:259–267, 1994

8. D.C. Alexander: Multiple-fiber reconstruction algorithms for diffusion MRI. Ann N Y Acad Sci 1064:113–133, 2005

9. D.K. Jones, M. Cercignani: Twenty-five pitfalls in the analysis of diffusion MRI data. NMR Biomed 23:803–820, 2010

10. D.C. Alexander, T.B. Dyrby, M. Nilsson, et al: Imaging brain microstructure with diffusion MRI: practicality and applications. NMR Biomed 32:e3841, 2019

11. J.H. Jensen, J.A. Helpern, A. Ramani, et al: Diffusional kurtosis imaging: the quantification of non-gaussian water diffusion by means of magnetic resonance imaging. Magn Reson Med 53:1432–1440, 2005

12. V.G. Kiselev: The Cumulant Expansion An Overarching Mathematical Framework For Understanding Diffusion NMR. Diffusion MRI 152–168, 2010

13. M. Descoteaux, R. Deriche, D. Le Bihan, et al: Multiple q-shell diffusion propagator imaging. Med Image Anal 15:603–621, 2011

14. J.-D. Tournier, S. Mori, A. Leemans: Diffusion tensor imaging and beyond. Magn Reson Med 65:1532–1556, 2011

15. S. Mori, B.J. Crain, V.P. Chacko, et al: Three-dimensional tracking of axonal projections in the brain by magnetic resonance imaging. Ann Neurol 45:265–269, 1999

16. F. Prados, I. Boada, A. Prats-Galino, et al: Analysis of new diffusion tensor imaging anisotropy measures in the three-phase plot. J Magn Reson Imaging 31:1435–1444, 2010

17. P.J. Basser: Inferring microstructural features and the physiological state of tissues from diffusion-weighted images. NMR Biomed 8:333–344, 1995

18. S. Mori, J. Zhang: Principles of diffusion tensor imaging and its applications to basic neuroscience research. Neuron 51:527–539, 2006

19. C. Beaulieu: The basis of anisotropic water diffusion in the nervous system - a technical review. NMR Biomed 15:435–455, 2002

20. C.A.M. Wheeler-Kingshott, M. Cercignani: About "axial" and "radial" diffusivities. Magn Reson Med 61:1255–1260, 2009

21. D.K. Jones, T.R. Knösche, R. Turner: White matter integrity, fiber count, and other fallacies: The do's and don'ts of diffusion MRI. NeuroImage 73:239–254, 2013

22. J.H. Jensen, J.A. Helpern: MRI quantification of non-Gaussian water diffusion by kurtosis analysis. NMR Biomed 23:698–710, 2010

23. E.X. Wu, M.M. Cheung: MR diffusion kurtosis imaging for neural tissue characterization. NMR Biomed 23:836–848, 2010

24. J. Veraart, D.H.J. Poot, W. Van Hecke, et al: More accurate estimation of diffusion tensor parameters using diffusion Kurtosis imaging. Magn Reson Med 65:138–145, 2011

25. B. Hansen, N. Shemesh, S.N. Jespersen: Fast imaging of mean, axial and radial diffusion kurtosis. Neuroimage 142:381–393, 2016

26. E.S. Hui, M.M. Cheung, L. Qi, E.X. Wu: Towards better MR characterization of neural tissues using directional diffusion kurtosis analysis. Neuroimage 42:122–134, 2008

27. D.H.J. Poot, A.J. den Dekker, E. Achten, et al: Optimal experimental design for diffusion kurtosis imaging. IEEE Trans Med Imaging 29:819–829, 2010

28. M.F. Falangola, J.H. Jensen, J.S. Babb, et al: Age-related non-Gaussian diffusion patterns in the prefrontal brain. J Magn Reson Imaging 28:1345–1350, 2008

29. S. De Santis, Y. Assaf, D.K. Jones: Using the biophysical CHARMED model to elucidate the underpinnings of contrast in diffusional kurtosis analysis of diffusion-weighted MRI. MAGMA 25:267–276, 2012

30. R. Neto Henriques, M.M. Correia, R.G. Nunes, et al: Exploring the 3D geometry of the diffusion kurtosis tensor--impact on the development of robust tractography procedures and novel biomarkers. Neuroimage 111:85–99, 2015

31. D.K. Jones: Diffusion MRI. Oxford University Press, 2010

32. B. Jeurissen, M. Descoteaux, S. Mori, et al: Diffusion MRI fiber tractography of the brain. NMR Biomed 32:e3785, 2019

33. J.-D. Tournier, F. Calamante, D.G. Gadian, et al: Direct estimation of the fiber orientation density function from diffusion-weighted MRI data using spherical deconvolution. Neuroimage 23:1176–1185, 2004

34. L.R. Frank: Characterization of anisotropy in high angular resolution diffusion-weighted MRI. Magn Reson Med 47:1083–1099, 2002

35. J.-D. Tournier, F. Calamante, A. Connelly: Robust determination of the fibre orientation distribution in diffusion MRI: non-negativity constrained super-resolved spherical deconvolution. Neuroimage 35:1459–1472, 2007

36. J.-D. Tournier, C.-H. Yeh, F. Calamante, et al: Resolving crossing fibres using constrained spherical deconvolution: validation using diffusion-weighted imaging phantom data. Neuroimage 42:617–625, 2008

37. D. Raffelt, J.-D. Tournier, S. Rose, et al: Apparent Fibre Density: a novel measure for the analysis of diffusion-weighted magnetic resonance images. Neuroimage 59:3976–3994, 2012

38. D.A. Raffelt, R.E. Smith, G.R. Ridgway, et al: Connectivity-based fixel enhancement: Whole-brain statistical analysis of diffusion MRI measures in the presence of crossing fibres. Neuroimage 117:40–55, 2015

39. D.A. Raffelt, J.-D. Tournier, R.E. Smith, et al: Investigating white matter fibre density and morphology using fixel-based analysis. Neuroimage 144:58–73, 2017

40. M. Palombo, A. Ianus, M. Guerreri, et al: SANDI: A compartment-based model for non-invasive apparent soma and neurite imaging by diffusion MRI. Neuroimage 215:116835, 2020

41. KL. Miller, CJ. Stagg, G. Douaud, et al: Diffusion imaging of whole, post-mortem human brains on a clinical MRI scanner. Neuroimage. 57(1):167-181, 2011

42. I.O. Jelescu, M. Palombo, F. Bagnato, et al: Challenges for biophysical modeling of microstructure. J Neurosci Methods 344:108861, 2020

43. Y. Assaf, R.Z. Freidlin, G.K. Rohde, et al: New modeling and experimental framework to characterize hindered and restricted water diffusion in brain white matter. Magn Reson Med 52:965–978, 2004

44. D.C. Alexander: A general framework for experiment design in diffusion MRI and its application in measuring direct tissue-microstructure features. Magn Reson Med 60:439–448, 2008

45. S. Santis, Y. Assaf, C.J. Evans, et al: Improved precision in CHARMED assessment of white matter through sampling scheme optimization and model parsimony testing. Magn Reson Med 71:661–671, 2014

46. Y. Assaf, T. Blumenfeld-Katzir, Y. Yovel, et al: AxCaliber: a method for measuring axon diameter distribution from diffusion MRI. Magn Reson Med 59:1347–1354, 2008

47. Y. Assaf, D.C. Alexander, D.K. Jones, et al: The CONNECT project: Combining macro- and micro-structure. Neuroimage 80:273–282, 2013

48. M. Tariq, T. Schneider, D.C. Alexander, et al: Bingham-NODDI: Mapping anisotropic orientation dispersion of neurites using diffusion MRI. Neuroimage 133:207–223, 2016

49. D. Barazany, P.J. Basser, Y. Assaf: In vivo measurement of axon diameter distribution in the corpus callosum of rat brain. Brain 132:1210–1220, 2009

50. H. Zhang, P.L. Hubbard, G.J.M. Parker, et al: Axon diameter mapping in the presence of orientation dispersion with diffusion MRI. Neuroimage 56:1301–1315, 2011

51. D.C. Alexander, P.L. Hubbard, M.G. Hall, et al: Orientationally invariant indices of axon diameter and density from diffusion MRI. Neuroimage 52:1374–1389, 2010

52. F. Sepehrband, D.C. Alexander, N.D. Kurniawan, et al: Towards higher sensitivity and stability of axon diameter estimation with diffusion-weighted MRI. NMR Biomed 29:293–308, 2016

53. E. Fieremans, J.H. Jensen, J.A. Helpern: White matter characterization with diffusional kurtosis imaging. Neuroimage 58:177–188, 2011

54. D.S. Novikov, J. Veraart, I.O. Jelescu, et al: Rotationally-invariant mapping of scalar and orientational metrics of neuronal microstructure with diffusion MRI. Neuroimage 174:518–538, 2018

55. E. Fieremans, A. Benitez, J.H. Jensen, et al: Novel white matter tract integrity metrics sensitive to Alzheimer disease progression. AJNR Am J Neuroradiol 34:2105–2112, 2013

56. I.O. Jelescu, M. Zurek, K.V. Winters, et al: In vivo quantification of demyelination and recovery using compartment-specific diffusion MRI metrics validated by electron microscopy. Neuroimage 132:104–114, 2016

57. N.D. Kelm, K.L. West, R.P. Carson, et al: Evaluation of diffusion kurtosis imaging in ex vivo hypomyelinated mouse brains. Neuroimage 124:612–626, 2016

58. H. Zhang, T. Schneider, C.A. Wheeler-Kingshott, et al: NODDI: practical in vivo neurite orientation dispersion and density imaging of the human brain. Neuroimage 61:1000–1016, 2012

59. A. Szafer, J. Zhong, J.C. Gore: Theoretical model for water diffusion in tissues. Magn Reson Med 33:697–712, 1995

60. F. Grussu, T. Schneider, C. Tur, et al: Neurite dispersion: a new marker of multiple sclerosis spinal cord pathology?. Ann Clin Transl Neurol 4:663–679, 2017

61. I.O. Jelescu, J. Veraart, E. Fieremans, et al: Degeneracy in model parameter estimation for multi-compartmental diffusion in neuronal tissue. NMR Biomed 29:33–47, 2016

62. E. Kleban, C.M.W. Tax, U.S. Rudrapatna, et al: Strong diffusion gradients allow the separation of intra- and extra-axonal gradient-echo signals in the human brain. Neuroimage 217:116793, 2020

63. B. Lampinen, F. Szczepankiewicz, J. Mårtensson, et al: Neurite density imaging versus imaging of microscopic anisotropy in diffusion MRI: A model comparison using spherical tensor encoding. NeuroImage 147:517–531, 2017

64. E. Kaden, F. Kruggel, D.C. Alexander: Quantitative mapping of the per-axon diffusion

coefficients in brain white matter. Magn Reson Med 75:1752–1763, 2016

65. E. Kaden, N.D. Kelm, R.P. Carson, et al: Multi-compartment microscopic diffusion imaging. Neuroimage 139:346–359, 2016

66. R.N. Henriques, S.N. Jespersen, N. Shemesh: Microscopic anisotropy misestimation in spherical-mean single diffusion encoding MRI. Magn Reson Med 81:3245–3261, 2019

67. D. Johnson, A. Ricciardi, W. Brownlee, et al. Comparison of Neurite Orientation Dispersion and Density Imaging and two-compartment Spherical Mean Technique parameter maps in multiple sclerosis. Front Neurol. 12, 2021

68. Y. Wang, Q. Wang, J.P. Haldar, et al: Quantification of increased cellularity during inflammatory demyelination. Brain 134:3590–3601, 2011

69. X. Wang, M.F. Cusick, Y. Wang, et al: Diffusion basis spectrum imaging detects and distinguishes coexisting subclinical inflammation, demyelination and axonal injury in experimental autoimmune encephalomyelitis mice. NMR Biomed 27:843–852, 2014

70. T.-H. Lin, C.-W. Chiang, C.J. Perez-Torres, et al: Diffusion MRI quantifies early axonal loss in the presence of nerve swelling. J Neuroinflammation 14:78, 2017

71. O. Pasternak, N. Sochen, Y. Gur, et al: Free water elimination and mapping from diffusion MRI. Magnetic Resonance in Medicine 62:717–730, 2009

72. O. Pasternak, C.-F. Westin, S. Bouix, et al: Excessive Extracellular Volume Reveals a Neurodegenerative Pattern in Schizophrenia Onset. Journal of Neuroscience 32:17365–17372, 2012

73. M. Dumont, M. Roy, P.-M. Jodoin, et al: Free water in white matter differentiates MCI and AD from control subjects. Front Aging Neurosci 11:270, 2019

74. A.R. Hoy, C.G. Koay, S.R. Kecskemeti, et al: Optimization of a free water elimination two-compartment model for diffusion tensor imaging. Neuroimage 103:323–333, 2014

75. A. Albi, O. Pasternak, L. Minati,et al: Free water elimination improves test–retest reproducibility of diffusion tensor imaging indices in the brain: A longitudinal multisite study of healthy elderly subjects. Human Brain Mapping 38:12–26, 2017

76. B. Scherrer, A. Schwartzman, M. Taquet, et al: Characterizing brain tissue by assessment of the distribution of anisotropic microstructural environments in diffusion-compartment imaging (DIAMOND). Magn Reson Med 76:963–977, 2016

77. B. Scherrer, M. Taquet, A. Schwartzman, et al: Decoupling Axial and Radial Tissue Heterogeneity in Diffusion Compartment Imaging. Information Processing in Medical Imaging Springer Cham 440–452, 2017

78. G. Rensonnet, B. Scherrer, S.K. Warfield, et al: Assessing the validity of the approximation of diffusion-weighted-MRI signals from crossing fascicles by sums of signals from single fascicles. Magn Reson Med 79:2332–2345, 2018

79. E.C. Parsons, M.D. Does, J.C. Gore: Temporal diffusion spectroscopy: Theory and implementation in restricted systems using oscillating gradients. Magnetic Resonance in

Medicine 55:75–84, 2006

80. M. Aggarwal, M.V. Jones, P.A. Calabresi, et al: Probing mouse brain microstructure using oscillating gradient diffusion MRI. Magn Reson Med 67:98–109, 2012

81. I. Drobnjak, H. Zhang, A. Ianuş, et al: PGSE, OGSE, and sensitivity to axon diameter in diffusion MRI: Insight from a simulation study. Magn Reson Med 75:688–700, 2016

82. M. Nilsson, S. Lasič, I. Drobnjak, et al: Resolution limit of cylinder diameter estimation by diffusion MRI: The impact of gradient waveform and orientation dispersion. NMR Biomed 30, 2017

83. N. Shemesh, S.N. Jespersen, D.C. Alexander, et al: Conventions and nomenclature for double diffusion encoding NMR and MRI. Magn Reson Med 75:82–87, 2016

84. M.A. Koch, J. Finsterbusch: Compartment size estimation with double wave vector diffusion-weighted imaging. Magn Reson Med 60:90–101, 2008

85. S. Nørhøj Jespersen, N. Buhl: The displacement correlation tensor: microstructure, ensemble anisotropy and curving fibers. J Magn Reson 208:34–43, 2011

86. P.P. Mitra: Multiple wave-vector extensions of the NMR pulsed-field-gradient spin-echo diffusion measurement. Physical Review B 51:15074–15078, 1995

87. G. Yang, J.A. McNab: Eddy current nulled constrained optimization of isotropic diffusion encoding gradient waveforms. Magn Reson Med 81:1818–1832, 2019

88. C.-F. Westin, H. Knutsson, O. Pasternak, et al: Q-space trajectory imaging for multidimensional diffusion MRI of the human brain. Neuroimage 135:345–362, 2016

89. F. Szczepankiewicz, D. van Westen, E. Englund, et al: The link between diffusion MRI and tumor heterogeneity: Mapping cell eccentricity and density by diffusional variance decomposition (DIVIDE). Neuroimage 142:522–532, 2016

90. M. Filippi, F. Agosta: Diffusion tensor imaging and functional MRI. Handbook of Clinical Neurology 1065–1087, 2016

91. S. Llufriu, E. Martinez-Heras, E. Solana, et al: Structural networks involved in attention and executive functions in multiple sclerosis. Neuroimage Clin 13:288–296, 2017

92. S. By, J. Xu, B. A Box, et al: Application and evaluation of NODDI in the cervical spinal cord of multiple sclerosis patients. NeuroImage: Clinical 15:333–342, 2017

93. D.A. Lakhani, K.G. Schilling, J. Xu, et al: Advanced Multicompartment Diffusion MRI Models and Their Application in Multiple Sclerosis. AJNR Am J Neuroradiol 41:751–757, 2020

94. E.M. Palacios, J.P. Owen, E.L. Yuh, et al: TRACK-TBI Investigators, The evolution of white matter microstructural changes after mild traumatic brain injury: A longitudinal DTI and NODDI study. Sci Adv 6:eaaz6892, 2020

95. Y. Kadota, T. Hirai, M. Azuma, et al: Differentiation between glioblastoma and solitary brain metastasis using neurite orientation dispersion and density imaging. J Neuroradiol

47:197–202, 2020

96. C. Andica, K. Kamagata, T. Hatano, et al: MR Biomarkers of Degenerative Brain Disorders Derived From Diffusion Imaging. J Magn Reson Imaging 52:1620–1636, 2020

97. M.A. Rocca, M.P. Amato, N. De Stefano, et al: MAGNIMS Study Group, Clinical and imaging assessment of cognitive dysfunction in multiple sclerosis. Lancet Neurol 14:302–317, 2015

98. M. Rovaris, F. Agosta, E. Pagani, et al: Diffusion Tensor MR Imaging, Neuroimaging Clinics of North America. 19:37–43, 2009

99. S. Llufriu, E. Martinez-Heras, J. Fortea, et al: Cognitive functions in multiple sclerosis: impact of gray matter integrity. Mult Scler 20:424–432, 2014

100. L.E. Jonkman, R. Klaver, L. Fleysher, et al: The substrate of increased cortical FA in MS: A 7T post-mortem MRI and histopathology study. Mult Scler 22:1804–1811, 2016

101. R. Rahmanzadeh, P.-J. Lu, M. Barakovic, M. Weigel, et al: Myelin and axon pathology in multiple sclerosis assessed by myelin water and multi-shell diffusion imaging. Brain, 2021

102. C. Thaler, A.A. Kyselyova, T.D. Faizy, et al: Heterogeneity of multiple sclerosis lesions in fast diffusional kurtosis imaging. PLoS One 16:e0245844, 2021

103. S. De Santis, M. Bastiani, A. Droby, et al: Characterizing Microstructural Tissue Properties in Multiple Sclerosis with Diffusion MRI at 7 T and 3 T: The Impact of the Experimental Design. Neuroscience 403:17–26, 2019

104. I. de Kouchkovsky, E. Fieremans, L. Fleysher, et al: Quantification of normal-appearing white matter tract integrity in multiple sclerosis: a diffusion kurtosis imaging study. J Neurol 263:1146–1155, 2016

105. S. Collorone, N. Cawley, F. Grussu, et al: Reduced neurite density in the brain and cervical spinal cord in relapsing-remitting multiple sclerosis: A NODDI study. Mult Scler 26:1647–1657, 2020

106. T. Schneider, W. Brownlee, H. Zhang, et al: Sensitivity of multi-shell NODDI to multiple sclerosis white matter changes: a pilot study. Funct Neurol 32:97–101, 2017

107. S. Collorone, F. Prados, B. Kanber, et al: Brain microstructural and metabolic alterations detected in vivo at onset of the first demyelinating event. Brain, 2021

108. F. Bagnato, G. Franco, H. Li, et al: Probing axons using multi-compartmental diffusion in multiple sclerosis. Ann Clin Transl Neurol 6:1595–1605, 2019

109. S. By, J. Xu, B.A. Box, et al: Multi-compartmental diffusion characterization of the human cervical spinal cord in vivo using the spherical mean technique. NMR Biomed 31:e3894, 2018

110. E. Martínez-Heras, E. Solana, F. Prados, et al: Characterization of multiple sclerosis lesions with distinct clinical correlates through quantitative diffusion MRI. Neuroimage Clin 28:102411, 2020

111. M. Yoshida, M. Hori, K. Yokoyama, et al: Diffusional kurtosis imaging of normal-appearing white matter in multiple sclerosis: preliminary clinical experience. Jpn J Radiol 31:50–55, 2013

112. P. Vilela, H.A. Rowley: Brain ischemia: CT and MRI techniques in acute ischemic stroke. European Journal of Radiology 96:162–172, 2017

113. Z. Wang, S. Zhang, C. Liu, et al: A study of neurite orientation dispersion and density imaging in ischemic stroke. Magn Reson Imaging 57:28–33, 2019

114. A. Mastropietro, G. Rizzo, L. Fontana, et al: Microstructural characterization of corticospinal tract in subacute and chronic stroke patients with distal lesions by means of advanced diffusion MRI. Neuroradiology 61:1033–1045, 2019

115. K. Hodgson, G. Adluru, L.G. Richards, et al: Predicting Motor Outcomes in Stroke Patients Using Diffusion Spectrum MRI Microstructural Measures. Frontiers in Neurology 10, 2019

116. W. Khan, N. Egorova, M.S. Khlif, et al: Three-tissue compositional analysis reveals in-vivo microstructural heterogeneity of white matter hyperintensities following stroke. Neuroimage 218:116869, 2020.

117. X. Fu, S. Shrestha, M. Sun, et al: Microstructural White Matter Alterations in Mild Cognitive Impairment and Alzheimer's Disease : Study Based on Neurite Orientation Dispersion and Density Imaging (NODDI). Clin Neuroradiol 30:569–579, 2020

118. T.D. Parker, C.F. Slattery, J. Zhang, et al: Cortical microstructure in young onset Alzheimer's disease using neurite orientation dispersion and density imaging. Hum Brain Mapp 39:3005–3017, 2018

119. G.-P. Song, T.-T. Yao, D. Wang, et al: Differentiating between Alzheimer's disease, amnestic mild cognitive impairment, and normal aging diffusion kurtosis imaging. Neural Regeneration Res 14:2141–2146, 2019

120. Y. Chen, M. Sha, X. Zhao, et al: Automated detection of pathologic white matter alterations in Alzheimer's disease using combined diffusivity and kurtosis method. Psychiatry Res Neuroimaging 264:35–45, 2017

121. K. Kamagata, C. Andica, T. Hatano, et al: Advanced diffusion magnetic resonance imaging in patients with Alzheimer's and Parkinson's diseases. Neural Regeneration Res 15:1590–1600, 2020

122. C.F. Slattery, J. Zhang, R.W. Paterson, et al: ApoE influences regional white-matter axonal density loss in Alzheimer's disease. Neurobiol Aging 57:8–17, 2017

123. G. Abdalla, L. Dixon, E. Sanverdi, et al: The diagnostic role of diffusional kurtosis imaging in glioma grading and differentiation of gliomas from other intra-axial brain tumours: a systematic review with critical appraisal and meta-analysis. Neuroradiology 62:791–802, 2020

124. C. Qi, S. Yang, L. Meng, et al: Evaluation of cerebral glioma using 3T diffusion kurtosis tensor imaging and the relationship between diffusion kurtosis metrics and tumor cellularity. J Int Med Res 45:1347–1358, 2017

125. X.-F. Wu, X. Liang, X.-C. Wang, et al: Differentiating high-grade glioma recurrence from pseudoprogression: Comparing diffusion kurtosis imaging and diffusion tensor imaging. Eur J Radio. 135:109445, 2021

126. S.-H. Li, R.-F. Jiang, J. Zhang, et al: Application of Neurite Orientation Dispersion and Density Imaging in Assessig Glioma Grades and Cellular Proliferation. World Neurosurg 131:e247–e254, 2019

127. J. Zhao, J.-B. Li, J.-Y. Wang, et al: Quantitative analysis of neurite orientation dispersion and density imaging in grading gliomas and detecting gene mutation status. Neuroimage Clin 19:174–181, 2018

128. S. Masjoodi, H. Hashemi, M.A. Oghabian, et al: Differentiation of Edematous, Tumoral and Normal Areas of Brain Using Diffusion Tensor and Neurite Orientation Dispersion and Density Imaging. J Biomed Phys Eng 8:251–260, 2018

129. J. Mao, W. Zeng, Q. Zhang, et al: Differentiation between high-grade gliomas and solitary brain metastases: a comparison of five diffusion-weighted MRI models. BMC Med Imaging 20:124, 2020